Journal of The Electrochemical Society, **160** (6) A793-A804 (2013)
0013-4651/2013/160(6)/A793/12/$31.00 © The Electrochemical Society

Failure Investigation of $LiFePO_4$ Cells in Over-Discharge Conditions

Hao He,[a,d] Yadong Liu,[a] Qi Liu,[a] Zhefei Li,[a] Fan Xu,[a] Clif Dun,[b] Yang Ren,[c] Mei-xian Wang,[a] and Jian Xie[a,*,z]

[a]*Department of Mechanical Engineering, Purdue School of Engineering and Technology, Indiana University-Purdue University, Indianapolis, Indiana 46202, USA*
[b]*School of Dentistry, Indiana University, Indianapolis, Indiana 46202, USA*
[c]*X-ray Science Division, Argonne National Laboratory, Argonne, Illinois 60439, USA*

The failure mechanism of $LiFePO_4$ cells in over-discharge conditions has been systematically studied using commercial A123 18650 cells at a 1.0 C rate and different conditions – from 5% to 20% over-discharge (DOD = 105% to 120%). SEM/EDAX, high-energy synchrotron XRD (HESXRD), and cyclic voltammetry (CV) were used to characterize the morphology, structure, and electrode potentials of cell components both in situ and ex situ. The failure behaviors of A123 18650 cells experiencing different degrees of over-discharge were found to be similar, and the 20% over-discharge process was analyzed as the representative example. The Cu electrochemical potentials in the 1.2 M $LiPF_6$ EC/EMC electrolyte were measured during the charge/over-discharge process using CV, proving that Cu oxidation and reduction in the cell during the charge/over-discharge cycle were theoretically possible to proceed. A possible failure mechanism is proposed: during the over-discharging process, Cu foil oxidized first to Cu^+, then to Cu^{2+} cations; next, these Cu^+ and Cu^{2+} cations diffused to the cathode side from the anode side; and finally, these Cu^{2+} cations reduced to Cu^+ cations, and then reduced further, back to metallic Cu. During charge/over-discharge cycling, Cu dendrites continued growing from the cathode side, penetrating through the separator and forming a copper bridge between the anode and cathode. The copper bridge caused micro-shorting and eventually led to the failure of the cell. During the charge/over-discharge cycles, the continued cell temperature increase at the end of over-discharge is evidence of the micro-shorting.
 [DOI: 10.1149/2.039306jes]

Manuscript submitted December 17, 2012; revised manuscript received February 28, 2013. Published March 13, 2013.

Driven by the environmental protection needs and the quickly increasing price of fossil fuels, the need for clean and high-efficiency energy conversion and storage devices has become more urgent than ever. Lithium-ion batteries, which were first commercially introduced into the market in 1991 by Sony,[1] are the best candidates for meeting such needs. The development of electric vehicles (EVs) and hybrid electric vehicles (HEVs) along with portable electronics (i.e. cell phones, laptops, etc.) demands batteries with high energy density and high efficiency. The Li-ion battery has proved to be a prominent energy storage device for HEVs and EVs due to its high specific energy and high specific power.[2]

In most applications of portable electronics, EVs, and HEVs, instead of a single cell, multiple cells of Li-ion batteries are used in battery packs, usually ranging from tens to hundreds or even thousands of cells, to supply the desired energy and power. However, when a number of $LiFePO_4$ cells are used in a battery pack, a capacity distribution band always exists because the capacity varies between the cells.[3,4] This capacity band will broaden with the cycle number, and eventually, the cell with the lowest capacity will limit the capacity of the battery pack. Thus, the lowest capacity cell will experience overcharge and over-discharge, even if the whole pack is experiencing normal charge/discharge cycles. With a battery management system, the capacity band of a battery pack can be controlled within a certain range, but the band cannot be eliminated. Thus, the cell is likely to cause some serious safety problems because Li-ion battery cells have very low tolerance to abuses including overcharge and over-discharge. Very often, over-discharge causes failure of the whole pack or may even cause a serious safety accident. Hence, understanding the behavior of $LiFePO_4$ cells in over-discharge and overcharge conditions is critical for the safety of $LiFePO_4$ cells.[5]

The safety of Li-ion batteries has become an important issue; and efforts have been dedicated to studying the behavior of Li-ion batteries under different operating conditions,[6–8] but few have concentrated on the failure mechanisms of Li-ion batteries in over-discharge conditions. In their modeling work, Arora and White[9] proposed that copper (as a current collector) be oxidized into ions in the over-discharge process and then redeposited as copper metal at the electrode following the charging process, forming Cu dendrites that could penetrate through the separator, causing the cell to fail due to an internal short. However, these proposed reactions were not supported by the experiment. Hossain and co-workers[10] investigated the behavior of Li-ion batteries (with MCMB or hard carbon composite anodes and $LiCoO_2$ cathodes) during over-discharge using a Li reference electrode and found that the cell failed to charge after 3 over-discharge cycles. They proposed (without experimental validation) that the possible failure cause could be the copper dissolution and transfer to the cathode. Tobishima and co-workers' study[11] revealed that both $LiCoO_2$ and $LiMn_2O_4$ cells failed after forced discharge, namely, over-discharge, to 250%. So far, the failure mechanism of the $LiFePO_4$ cell in over-discharge conditions is still not clear.

In this work, the failure of $LiFePO_4$ cell in over-discharge conditions was systematically investigated. The commercial $LiFePO_4$ 18650 cells (A123 Systems) were chosen to be cycled under both normal and over-discharge conditions until failure. The failed cells along with the pristine cells were characterized using SEM for the morphology and composition changes. The cells were in situ characterized using synchrotron X-ray diffraction (XRD) for the electrode structural changes during cycling. The electrode potentials of the $LiFePO_4$ cathode, the graphite anode, and the cell voltage during cycling in an 18650 cell were in situ monitored using Li metal as the reference electrode. Finally, the failure mechanism of the $LiFePO_4$ Li-ion battery cell in over-discharge conditions was proposed with experimental validation.

Experimental

Failure of $LiFePO_4$ cells by over-discharge.— Materials.—All chemicals were used as received. The commercial cells chosen for this study were A123 18650 $LiFePO_4$ cells (APR18650M 1A 3.3 V 1100 mAh) from A123 Systems (Cambridge, MA), and $LiPF_6$, EC, and EMC from Novolyte (Cleveland, OH). Each cycling test was repeated on at least three different cells to ensure data reproducibility.

Electrochemical apparatus.—All potentials used in this paper were versus Li/Li^+ electrode potential unless otherwise noted. Over-discharge tests were carried out in a homemade explosion-proof chamber using both the BT-5000 8-channel battery and the BT-2000 32-channel cycler with a temperature-control sensor (Arbin Instruments, TX). Galvanostat tests were performed on the A123 18650 $LiFePO_4$ cells with a nominal 1100-mAh capacity. The cells were charged to

*Electrochemical Society Active Member.
[d]Present address: Hunan University, Changsha City, Hunan Province 410082, China.
[z]Email: jianxie@iupui.edu

3.60 V at a 1 C rate (constant current of 1.10 A) first; then, the charging was continued at a constant voltage of 3.60 V until the current was < 0.02 A, which is regarded as a 100% state of charge (SOC) or 0% depth of discharge (DOD). After a short rest (i.e. 5 min.), the cell was discharged at a 1 C rate until the voltage reached 2.00 V, which is the discharge cutoff voltage of the cell (the corresponding capacity is 1100 mAh). This procedure is considered to be a 100% depth of discharge (DOD). The over-discharge test conditions were carried out at a 1 C rate (constant current,1.10A) and based on the Coulombs discharged out of the cell; namely, the discharge step was terminated when the cells reach 105% DOD (63 min., 1155 mAh), 110% DOD (66 min., 1210 mAh), 115% DOD (69 min., 1265 mAh), and 120% DOD (72 min., 1320 mAh) instead of 2.00 V while the cell voltage went negative at the end of over-discharge. A thermocouple was placed on the skin of the A123 18650 $LiFePO_4$ cell at the middle of the cell and the temperature was measured simultaneously with the voltage during the cycling test. The charge/over-discharge cycle kept running until the cells failed. Current–voltage–temperature data were recorded every 5s during charge/over-discharge cycles.

Measurement of potentials of each electrode during testing for A123 18650 $LiFePO_4$ cells.— The head and bottom of the case of a fresh A123 18650 $LiFePO_4$ cell were carefully removed in the argon filled glove box using a roller cutter. The roll of assembly of the 18650 $LiFePO_4$ cell was placed into a container and immersed in the electrolyte. A lithium strip was inserted into this container and served as the reference electrode. The electrolyte was made with a 1.2 M $LiPF_6$ in EC-EMC (3:7) and 30 mL of the electrolyte was used to ensure complete immersion of the roll of the assembly. The same normal cycle and 20% over-discharge conditions mentioned in Electrochemical apparatus part of Experimental were employed in this experiment with the anode as the counter electrode, the cathode as the working electrode, and the Li metal as the reference electrode. The potentials of the anode and cathode and the voltage of the whole cell were measured separately by an 8 channel Solartron 1470E Multistat (Solartron, England).

Half-cell cyclic voltammogram (CV) test.— To study the reduction potentials of Cu in the electrolyte of 1.2 M $LiPF_6$ in EC-EMC (3:7), two different working electrodes were used: 1) a Pt wire electrode (99.99%, Fisher Scientific, NH), and 2) a pure Cu electrode (99.99%, CH Instruments, Inc., TX). The Pt metal foil served as the counter electrode, and the Li metal strip served as the reference electrode. Sandpaper and a 0.05 μm alumina suspension were employed to fully clean and remove the oxidation layer of the working electrodes. The potential window for cyclic voltammetry was set from −0.4 V to 5.0 V (or otherwise determined according to the anode and cathode potentials obtained in the experiment described earlier) with a scan rate of either 20 mV/s or 2 mV/s using a Solartron 1470E Multistat (Solartron, England). Before CV measurement, a 200-cycle scan with a scan rate of 1 V/s between 0–5 V was used to clean the surface of the working electrodes.

First, a cell using Pt metal as both the working and counter electrodes and Li metal as the reference electrode was used to study if there were any oxidation/reduction reactions from 1.2 M $LiPF_6$ or EC-EMC (3:7). Second, a Cu electrode was used as the working electrode, Pt foil as the counter electrode, and a Li metal strip as the reference electrode to study the behavior of Cu oxidation and reduction in 1.2 M $LiPF_6$ or EC-EMC (3:7) electrolyte.

SEM and EDAX characterization of 18650 $LiFePO_4$ cells.— The pristine and failed cells were carefully disassembled in the argon filled glove box using the same procedure as in Measurement of potentials of each electrode during testing for 123 A123 18650 $LiFePO_4$ cells part of Experimental to examine the morphology and composition of the electrodes and the separator. The samples were cut from the middle of the anode, cathode, and separator for SEM and EDAX (JEOL JXA-8900R) examination. The morphology, microstructure, and elements in these samples were analyzed using SEM and EDAX.

In-situ high-energy synchrotron X-ray diffraction (HESXRD) investigation of the behavior of A123 18650 $LiFeO_4$ cells during the 10% over-discharge process.— The high-energy synchrotron beamline of the Advanced Photon Source 11-ID-C (Argonne National Laboratory, IL) with a fixed high-energy X-ray beam ($\lambda = 0.10798$ Å, E = 115 keV, a beam size of 0.2 mm × 0.2 mm) was used to in-situ monitor the crystalline phase changes of A123 18650 $LiFeO_4$ cells during charge/over-discharge cycles. An A123 18650 $LiFeO_4$ cell was placed on the stage of the beamline and the high-energy synchrotron beam was penetrated through the cell while the cell was cycled using a Maccor battery test system (Tulsa, OK) with the same charge/over-discharge protocol mentioned in Electrochemical apparatus part of Experimental, while two dimensional (2D) diffraction patterns of the corresponding crystalline phases of each component in the cell (i.e. graphite, $LiFePO_4$, and stainless steel case) were recorded simultaneously during cycling. The data collection rate was one pattern per 30 seconds. The 2D data has been integrated to yield the one-dimensional high-energy synchrotron XRD (1D- HESXRD) patterns by FIT2D software.[12] The peak intensities were normalized to the monitor counts of the X-ray beam. Only the 1D-HESXRD data of the last cycle right before failure is shown in this paper.

Results and Discussion

Behavior of lithium-ion $LiFePO_4$ cells in over-discharge conditions.— A systematic approach was taken to investigate the effects of different depths of discharge (DODs) in the over-discharge process on the cycle performance of A123 $LiFePO_4$ 18650 cells. For comparison, A123 18650 $LiFePO_4$ cells were cycled under normal conditions (100% DOD) at a 1 C rate and room temperature. Under such conditions, the A123 $LiFePO_4$ 18650 cells showed excellent cycle performance and achieved 1750 cycles with 80% capacity and 2600 cycles with 60% capacity (Fig. 1a), respectively. However, the over-discharge process had a significant impact on cycle performance. When the DOD = 105%, 110%, 115%, and 120%, the cell failed after 110 cycles, 10 cycles, 3 cycles, and 2 cycles, respectively, as shown in Fig. 1b. When a cell cannot be charged/discharged, the cell is defined as failed. A great impact can be seen after 20% over-discharge—the cycle number dropped to 1 cycle. It was found that the failure phenomenon in the over-discharge process showed a consistent similar trend for the cells cycled with different DODs. In this paper, typical over-discharge process, 120% and 110% DOD (20% and 10% over-discharge), were chosen for the detailed analysis to elucidate the failure mechanism and provide a fundamental understanding of the relationship between the performance, temperature, and microstructure changes of the A123 18650 cell in the over-discharge process.

The cycle performance of A123 18650 $LiFePO_4$ cells under normal cycle conditions is shown in Fig. 2a for the charge/discharge voltage curves and temperature curves of the first three cycles. Under normal conditions, the charge plateau (3.4 V) and discharge plateau (3.12 V) can be clearly seen. There is only a 0.8∼1.2°C cell skin temperature increase at the end of the constant current charge process and a 0.7∼1.0°C decrease at the end of the constant potential charge process. A sharp temperature increase (2.1∼2.5°C) was observed at the end of the constant current discharge process.

The A123 18650 $LiFePO_4$ cells were also cycled under over-discharge conditions (5%, 10%, 15%, and 20% over-discharge). The charging/discharging curves and temperature curves for 120% DOD are shown in Fig. 2b. Under these conditions, the cell failed at the 2nd cycle. During the over-discharge process of the 1st cycle, the cell voltage dropped sharply from 2.00 V to as low as approximately −1.40 V, and then went back to −0.6 V and stayed around −0.6 V during the short resting period (i.e. 5 min.) while the surface temperature of the cell rose to 40°C at the end of over-discharge and stayed at 40°C during the short resting period. Compared with the cell under normal charge/discharge cycles, at the end of discharge, there was about a 3.7°C temperature increase for the cell at the end of over-discharge (36.3°C vs. 40.0°C). This suggests that some exothermic reactions

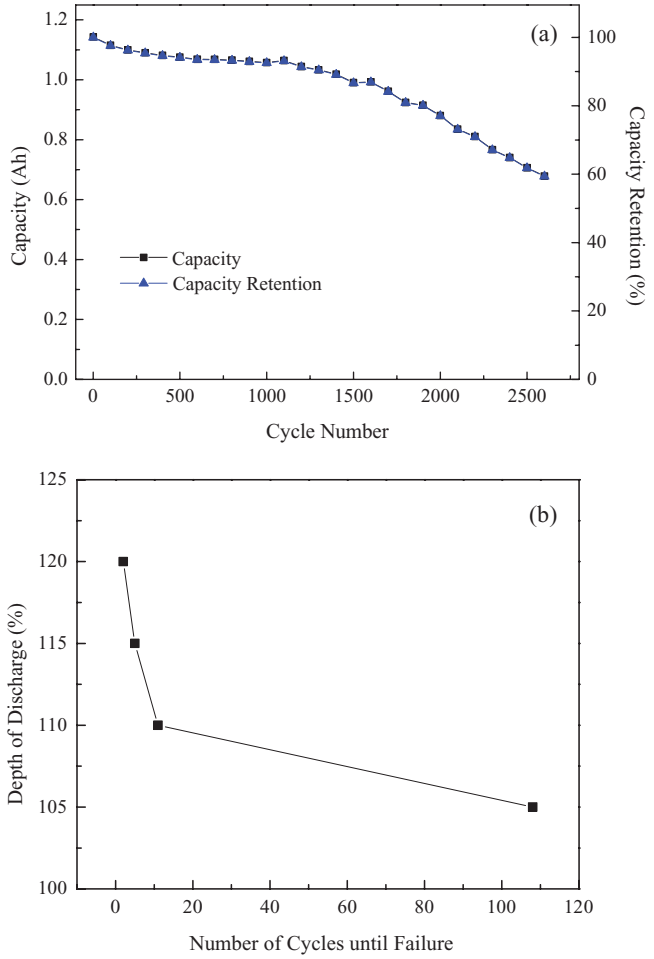

Figure 1. (a) Capacity and capacity degradation of an A123 18650 cell with cycle numbers under normal charge/discharge conditions at a 1 C rate; (b) the effect of DOD on the cycle life of an A123 18650 cell at a 1 C rate.

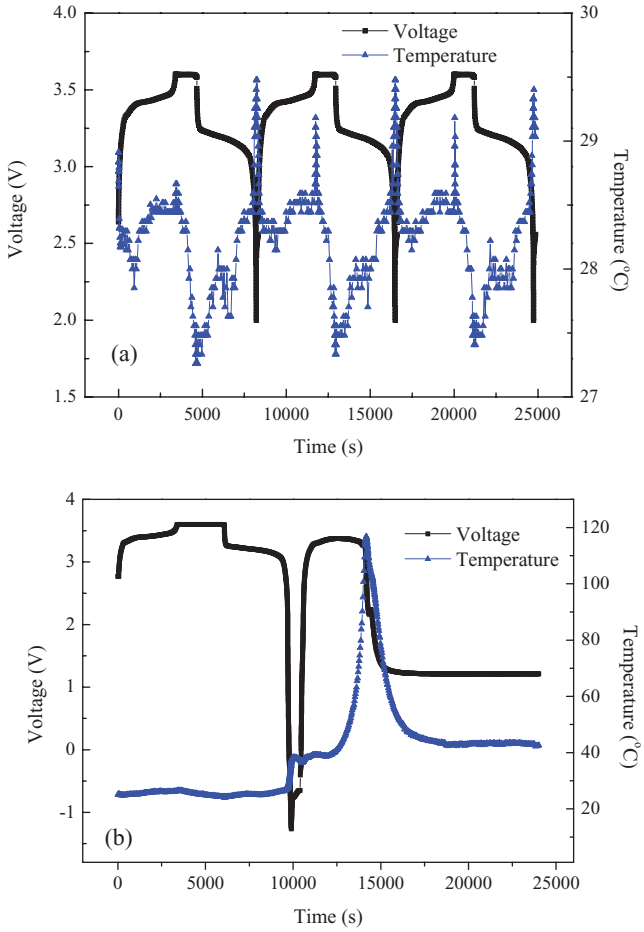

Figure 2. (a) Voltage and temperature changing over time of an A123 18650 cell under normal charge/discharge conditions; and (b) the charge/discharge voltage and temperature curves of an A123 18650 cell during over-discharge conditions (120% DOD, 20% over-discharge).

occurred during the over-discharge process. In the next charge process, the cell voltage could not go beyond 3.50 V, and then sharply dropped to 1.20 V. However the temperature increased sharply from 40°C to 120°C, then dropped to 40°C, while the cell voltage dropped to 1.20 V. This phenomenon implies that the cell might have micro-shorted and produced a large quantity of heat.

Since the cell cycled under 120% DOD and over-discharge lasted only for two cycles, it was difficult to observe the cell performance changes. Hence, the data of an A123 18650 $LiFePO_4$ cell experiencing 110% DOD over-discharge is shown in Fig. 3. The cell charge and discharge temperatures and voltages during the cycle are shown in Fig. 3a & 3b. The temperature at the end of the over-discharge process increased with the cycle number at a rate of 2.30°C/cycle and reached the maximum value, 47.45°C, right before the failure (Fig. 3a), while the temperature at the end of the normal discharge process remained constant, 29.50°C (Fig. 2a). From a controls perspective, clearly, the temperature increase at the end of discharge with the cycle number can be used as a signature for incoming cell failure. During the 10% over-discharge cycling, the cell temperature reached 31.19°C (at the end of 3rd charge process in Fig. 3a), the minimum value at the end of the charge process, and the temperature at the end of the charge also increased with the cycle number, but at a much slower rate, 0.67°C/cycle (Fig. 3a), suggesting that an internal-shorting was developing in the charge/over-discharge cycle and the heat generation rate inside the cell was increasing during the over-discharging process with the cycle number. The cell voltage at the end of the over-discharge process went to negative (Fig. 3b) due to the forced discharge, reached the maximum absolute value at the 2nd cycle (−1.13 V), and then increased with the cycle number, suggesting that an internal short was developing. This made the forced over-discharge more difficult, and the internal short was micro-shorting as evidenced by the slow increase of temperature with cycle number. The same pattern repeated with cycle number for each cycle, and the temperature continued to increase until failure (Fig. 3a). Taking a closer look at the temperature curves of a cycle (6th cycle, shown in Fig. 3c), the cell-skin temperature decreased with the time in the charging process at a rate of −0.23°C/min., but began a sharp increase during over-discharge with a rate of 0.9°C/min., indicating that the over-discharge caused detrimental damage to the cell components. This sharp temperature rise occurred only during the short period of over-discharge, suggesting that micro-shorting was developing during over-discharge. Overall, the increase of cell skin temperature with cycle number suggests that an internal shorting of the cell was developing with over-discharging, which eventually led to the failure. Fig. 3d shows the cell discharge capacity and capacity decay with cycles of charge/over-discharge. The data of the cell temperature at the end of over-discharge are also included for comparison. The capacity decreased at the rate of 0.067 (mAh/g)/cycle, while the cell temperature increased at the rate of 2.3°C/cycle, suggesting that a micro-short was developing and led to a decreased capacity, while the micro-shorting caused heat generation inside the cell that led to the temperature increase. It is well known that the abnormal operation of a Li-ion cell can result in the

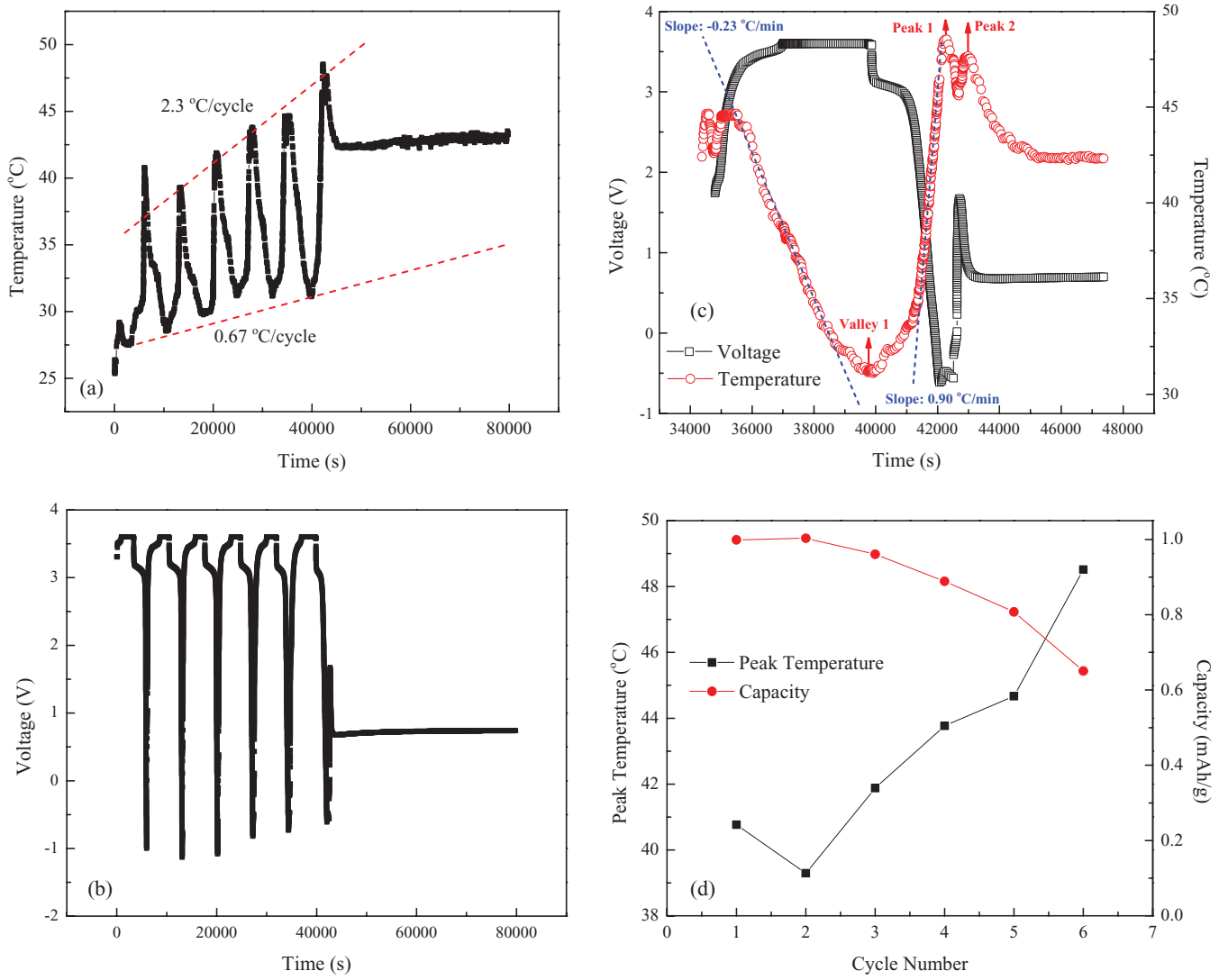

Figure 3. (a) Cell surface temperature, (b) cell voltage, (c) cell temperature and voltage of the 7th cycle (right before failure) of 10% over-discharge vs. time and (d) capacity vs. time in the over-discharge test of an A123 18650 $LiFePO_4$ cell (1.10 Ah) at a 1 C rate; cycling conditions: normal charge, then over-discharge (110% DOD, 10% over-discharge).

destruction and reformation of the anode SEI layer[13] as well as the cathode electrolyte interface (CEI),[14] especially at elevated temperatures. Therefore, the changes of the temperature, the voltage, and the capacity of a cell can be attributed to the related reactions and the microstructure changes of the cell components inside the cell during the over-discharge process. The change of SEI and CEI during the over-charge and over-discharge are under investigation and will be reported later. It is worthwhile to point out that the failure behavior of the A123 18650 $LiFePO_4$ cell under over-discharge is very similar to the failure behavior of the A123 18650 $LiFePO_4$ cell under overcharge, which we published in this journal (see Ref. 15), suggesting that the failure mechanism may be similar as well.

In-situ monitoring of the potential of the anode and cathode and the cell voltage of $LiFePO_4$ cells.— The detailed information of battery component changes during the over-discharge process is important for us to be able to understand the failure mechanism of the cell. In order to determine the potential change of each electrode under over-discharge conditions, a 3-electrode cell with Li metal as the reference electrode was used to measure the potentials of the cathode and the anode separately. The head and bottom of the case of an A123 18650 $LiFePO_4$ cell were carefully removed, and the core of the cell assembly (i.e. cathode, anode, and separator) was immersed into an electrolyte with a lithium strip serving as the reference electrode. In-situ monitoring of the anode and cathode potentials and the cell voltages of such a cell were measured for both normal cycling and over-discharge cycling. A normal cycle and a subsequent over-discharge cycle were carried out in such a 3-electrode cell and the potential profiles of each electrode and cell voltage of the 3-electrode cell are shown in Fig. 4. During the normal cycle (Fig. 4a), the potential of the cathode increased from 3.30 V (at the beginning of the charge) to 3.80 V (at the end of the charge) corresponding to the de-intercalation of the Li ions from the $LiFePO_4$ cathode, then decreased to 3.28 V at the end of the discharge. Meanwhile, the potential of the anode decreased from 0.65 V at the beginning of the charge to 0.23 V at the end of the charge, corresponding to the intercalation of the Li ions into graphite, then increased to 0.86 V at the end of discharge. Fig. 4b shows typical curves of the anode and cathode potentials and the cell voltages of the whole cell vs. time in a 20% over-discharge (120% DOD) process. The potentials of the anode and cathode as well as the cell voltage in the charging process changed in the same patterns as in a normal cycle; but by the end of the over-discharge process, the anode potential sharply

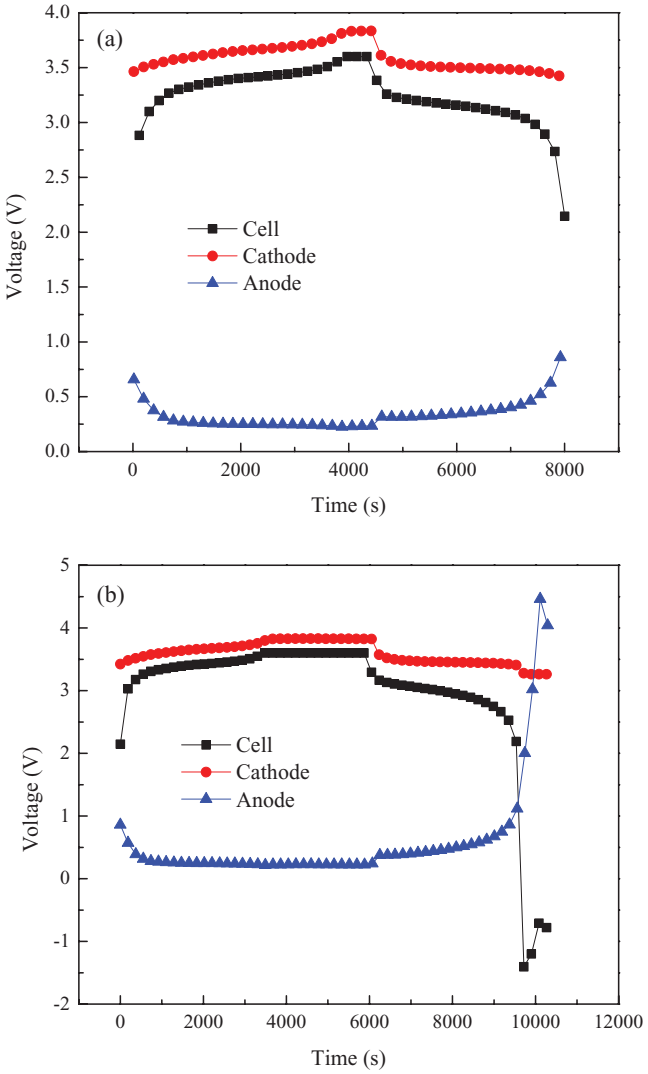

Figure 4. (a) Potential variation of anode and cathode and cell voltages vs. time during a normal charge/discharge cycle and (b) a charge / over-discharge cycle of a three-electrode A123 18650 $LiFePO_4$ cell (1.10 Ah) with a Li strip as the reference electrode at 1 C rate.

increased positively, to 4.50 V, and then dropped down to 4.00 V, while the cathode potential decreased to 3.16 V. At the end of the over-discharge process, the positive shift of the anode potential from 0.86 V (normal charge) to 4.50 V (20% over-discharge) suggests that some oxidation reactions may take place on the anode, while the shift of the cathode potential from 3.28 V (normal discharge) to 3.16 V indicates that some reduction reactions may occur at the cathode.

Electrochemical characterization of the possible copper corrosion process during the over-discharge process.— As mentioned above, the potential of each electrode could shift either positively or negatively during the over-discharge period, and oxidation and reduction could occur at the cathode and anode, respectively. One of the possibilities is that, in a cycle, Cu as the anode current collector could be oxidized at the anode and subsequently reduced at the cathode to form dendrites during the charging and over-discharging processes, respectively, causing an internal short. To determine whether this Cu oxidation and reduction occurs at the anode and cathode respectively, and since all electrochemical reactions are essentially controlled by the electrochemical potentials of the species, it is necessary to determine the potentials of reduction and oxidation of Cu/Cu^{2+} in the $LiPF_6$/EC-EMC electrolyte system to provide a fundamental understanding of the thermodynamic feasibility of the Cu/Cu^{2+} reduction and oxidation reactions. To obtain these potentials of Cu in the $LiPF_6$/EC-EMC electrolyte system, a systematic approach was taken. The potential window of the $LiPF_6$/EC-EMC electrolyte system was determined using a Pt working electrode first, to exclude any reduction or oxidation from the electrolyte system; then, a Cu working electrode was used to observe the oxidation and reduction potentials of Cu in the electrolytes. The CV curves obtained from different types of working electrodes are (1) Pt electrode and (2) pure Cu electrode in the $LiPF_6$/EC-EMC electrolyte system and are shown in Fig. 5a to 5c, respectively. An overall comparison of CV curves is shown in Fig. 5d. The baseline CV of $LiPF_6$/EC-EMC electrolyte was obtained using Pt as the working electrode and is shown in Fig. 5a. Clearly, no obvious reduction or oxidation peaks appeared in the entire potential range from −0.50 V to 4.5 V, indicating that the $LiPF_6$/EC-EMC electrolyte system is electrochemically stable within this potential window. When the Pt working electrode was replaced with a Cu electrode, the result was dramatically different (Fig. 5b). Two pairs of reversible redox couples appeared in the CV curve (Fig. 5b), which is identified with enlarged CV cures, 3.19 V/3.92 V and 3.28 V/4.17 V (Fig. 5c). From Fig. 5b and 5c, it is easily identified that the reduction potential of Cu^{2+} ions is around 3.28 V, while the reduction potential of Cu^{+} ions is around 3.19 V. The potentials of oxidation of Cu^{+} and Cu^{2+} ions can be determined from Fig. 5b and 5c, and the reduction potential of possible $Cu^{2+} + e^{-} \rightarrow Cu^{+}$ is around 3.28 V, while the reduction potential of $Cu^{+} + e^{-} \rightarrow Cu$ is around 3.19 V. From Fig. 5b and 5c, it can be concluded that the Cu metal oxidized to become Cu^{+} at 3.92 V ($Cu \rightarrow Cu^{+} + 1e^{-}$); then, the Cu^{+} further oxidized to become Cu^{2+} at 4.17 V ($Cu^{+} \rightarrow Cu^{2+} + 1e^{-}$); when the potential scanned back to negative direction, Cu^{2+} reduced to Cu^{+} at 3.28 V ($Cu^{2+} + 1e^{-} \rightarrow Cu^{+}$), then it further reduced to Cu metal at 3.19 V ($Cu^{+} + 1e^{-} \rightarrow Cu$). The detailed Cu/Cu^{+} and Cu^{+}/cu^{2+} oxidation/reduction processes in the $LiPF_6$/EC-EMC electrolyte system during the over-discharge and charge processes can be proposed based on the Cu/Cu^{+}, Cu^{+}/Cu^{2+} oxidation/reduction potentials, as shown in Fig. 6. The possible copper reduction/oxidation reactions in the electrolyte are listed below:

$$\text{Oxidation}: \quad Cu \rightarrow Cu^{+} + e^{-} \quad 3.92\,V\,(\text{vs. Li/Li}^{+}); \qquad [1]$$

$$\text{Reduction}: \quad Cu^{+} + e^{-} \rightarrow Cu \quad 3.19\,V\,(\text{vs. Li/Li}^{+}); \qquad [2]$$

$$\text{Oxidation}: \quad Cu^{+} \rightarrow Cu^{2+} + e^{-} \quad 4.17\,V\,(\text{vs. Li/Li}^{+}); \qquad [3]$$

$$\text{Reduction}: \quad Cu^{2+} + e^{-} \rightarrow Cu^{+} \quad 3.28\,V\,(\text{vs. Li/Li}^{+}); \qquad [4]$$

A potential chart (as shown in Fig. 6) was built to schematically show the potential change of each electrode during the charge/discharge process. In the charging process of a normal charge/discharge cycle, as seen in Fig. 6a, the cathode potential increased from 3.30 V to 3.80 V (also seen in Fig. 4a); in this process, neither the oxidation of Cu to Cu^{+} (3.92 V vs. Li/Li^{+}, reaction 1) nor further oxidation of Cu^{+} to Cu^{2+} (4.17 V vs. Li/Li^{+}, reaction 3) occurs on the cathode because the cathode potential is only 3.80 V (vs. Li/Li^{+}), which is less than the oxidation potentials of Cu to Cu^{+} (3.92 V) and Cu^{+} to Cu^{2+} (4.17 V), respectively. In addition, the cathode current collector is Al foil rather than Cu foil. The only possible reactions are Fe oxidations, which are unlikely to occur due to the source of Fe metal and have been discussed in great detail in our previous work.[13] On the other hand, in the charging process of a normal charge/discharge process, the anode potential decreased from 0.65 V to 0.23 V (also seen in Fig. 4a), and if there are any Cu^{+} or Cu^{2+} ions at the anode side, they could be reduced into Cu^{+} or Cu metal, respectively. In the following discharge process (Fig. 6b), the cathode potential decreased from 3.83 V to 3.28 V (also seen in Fig. 4b). The only possible reaction on the cathode is the reduction of

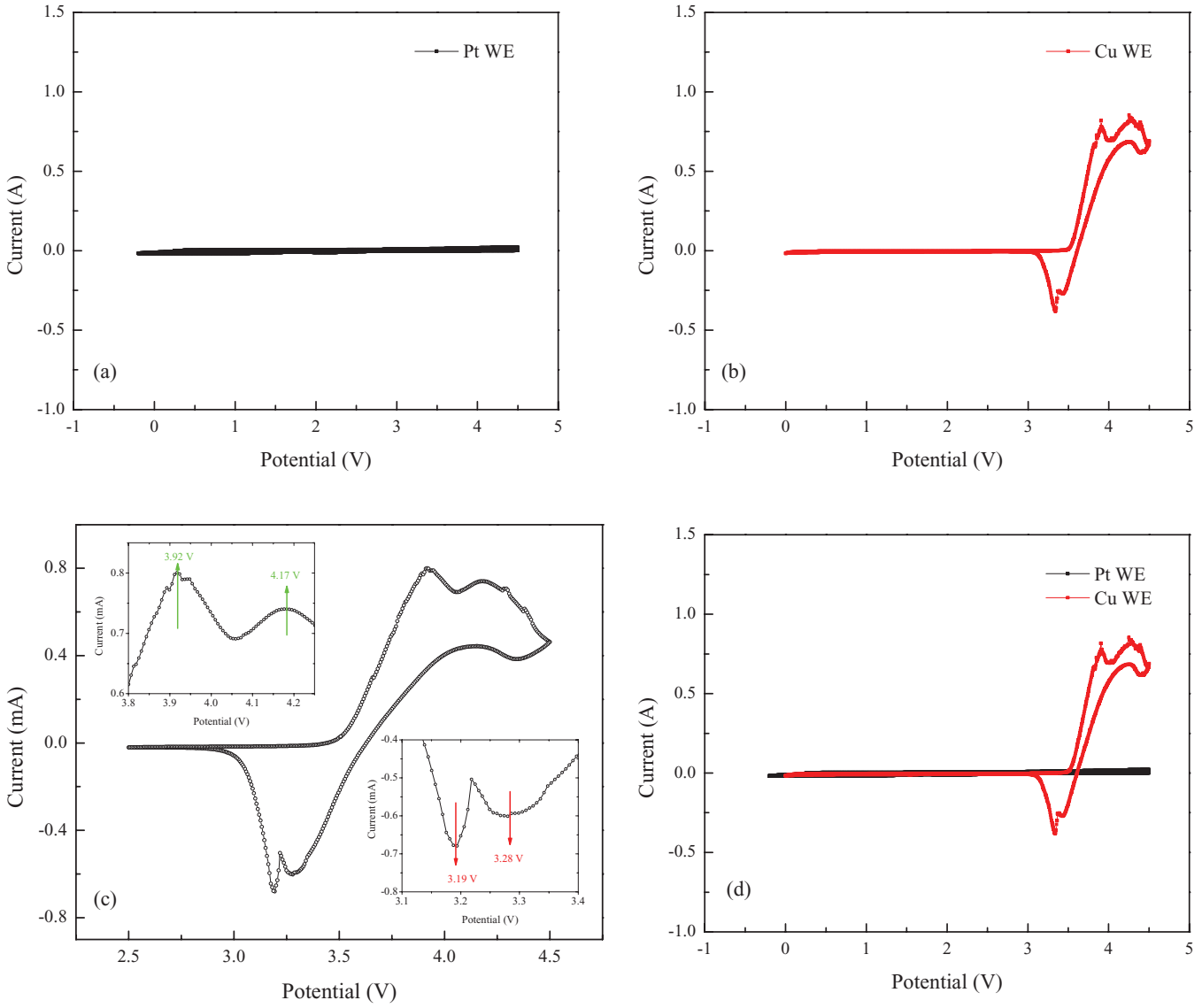

Figure 5. Cyclic voltammograms (CVs) of different metals in a $LiFP_6$ electrolyte (1.20 M $LiPF_6$ in EC-EMC (3:7)). (a) CV of Pt in a $LiFP_6$ electrolyte, working and counter electrodes: Pt; reference electrode: Li strip, potential range: 0.00 V to 4.50 V (vs. Li/Li^+), (b) CVs of Cu in a $LiFP_6$ electrolyte, WE: Cu, CE: Pt, and RE: Li, potential range: 0.00 V to 4.50 V (vs. Li/Li^+), (c) CVs of Cu in $LiFP_6$ electrolyte, WE: Cu, CE: Pt, and RE: Li, potential range: 2.50 V to 4.50 V (vs. Li/Li^+), and (d) CVs of combination of a, b, and c. All CVs were run at a scan rate of 2.0 $mV \cdot s^{-1}$.

Cu^{2+} ions to Cu^+ ions (3.28 V vs. Li/Li^+, reaction 4), not the reduction of Cu^+ ions to Cu metal (3.19 V vs. Li/Li^+, reaction 2). Hence, the oxidation of Cu foil (the anode current collector) should not occur during the normal charge/discharge cycles; consequently, nor should the Cu reduction occur at the cathode because no Cu^{2+} or Cu^+ ion sources were produced from the oxidation. However, in the normal charge and 20% over-discharge cycles, the situation is different. In the charging process of the 20% over-discharge/charge cycle, shown in Fig. 6c, the cathode potential increased from 3.18 V to 3.83 V while the anode potential decreased from 0.86 V to 0.23 V, and the possible reactions on both anode and cathode are similar to those in a normal charge/discharge cycle. In the following 20% over-discharge process, shown in Fig. 6d, the anode potential increased from 0.36 V to 4.50 V (also seen in Fig. 4b), and reactions 1 and 3 sequentially occurred; namely, metallic Cu (anode current collector) was oxidized to Cu^+ at 3.92 V, then Cu^+ was further oxidized into Cu^{2+} at 4.17 V at the anode and, finally, these Cu^{2+} ions transferred through the separator to the cathode side by diffusion. Simultaneously, the cathode potential decreased from 3.80 V to 3.16 V and reduction reactions 2 and 4 sequentially proceeded; namely, Cu^{2+} was reduced to Cu^+ at 3.28 V and Cu^+ was further reduced to Cu metal at 3.19 V. In the next over-discharge/charge cycle, the Cu current collector was oxidized again on the anode side and reduced on the cathode side. The same process repeated with the cycle number of the over-discharge/charge cycles, and the Cu dendrites grew from the cathode side and, eventually, the Cu dendrites penetrated through the separator and touched the anode to cause the internal short. Compared with the discharge processes in normal cycles, reactions 1 and 3 could not take place at the anode because the anode potential reached only 0.86 V (Fig. 5b) and never reached 4.20 V (Fig. 5d and Fig. 4b). This demonstrates that under normal cycling conditions, no Cu^+ or Cu^{2+} ions should be produced at the anode. Hence, there are no sources of Cu^+ or Cu^{2+} ions and consequently, the reductions of Cu^+ or Cu^{2+} ions could not occur at the cathode, and neither could the Cu dendrites. Therefore, the Cu dendrites could not be the root cause of the failure for $LiFePO_4$ cells under normal cycling conditions, which explains why these $LiFePO_4$

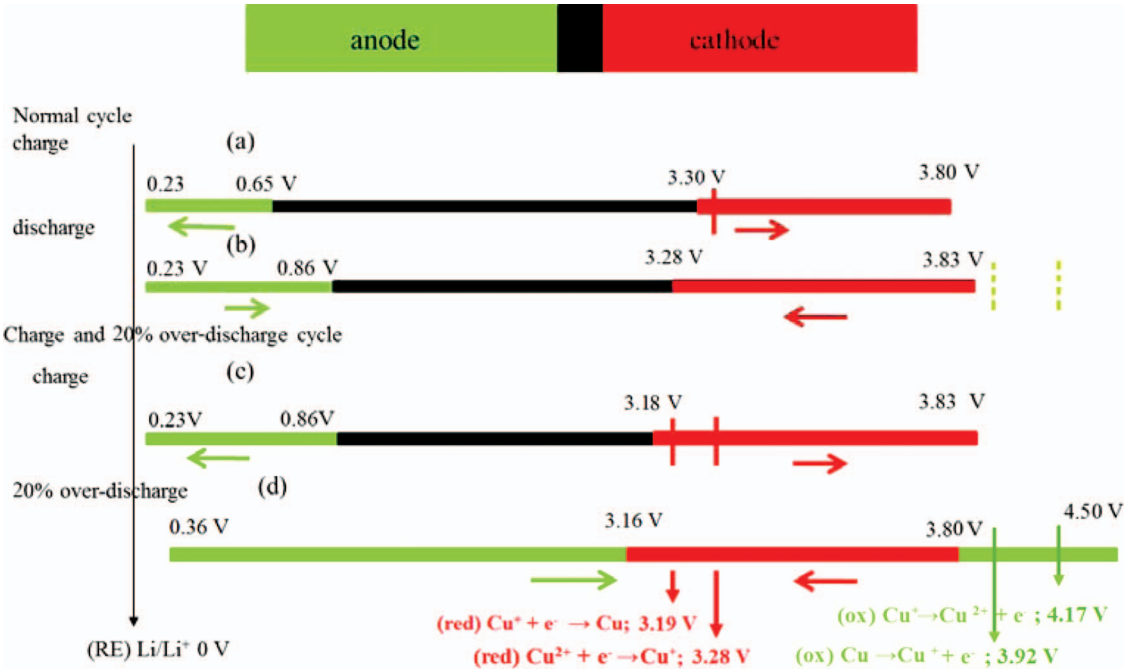

Figure 6. Schematic representation of electrode potential of anode and cathode change of an A123 18650 $LiFePO_4$ cell during each process: anode and cathode potential change (a) during the charging process and (b) during the discharging process of a normal charge/discharge cycle. Anode and cathode potential change (c) during the normal charging process and (d) during over-discharge process of a cycle of the normal charge and 20% over-discharging cycle. All electrochemical potentials regarding to the reduction potentials of Li/Li^+ (vs. Li/Li^+).

cells have an excellent cycle life, more than 1750 cycles with an 80% initial capacity (Fig. 1a).

High-energy synchrotron X-ray diffraction (HESXRD) investigation.— In order to further study the effects of the over-discharge process on the failure of the cell, and, in particular, on the material failure, the HESXRD technique was used to monitor the crystalline phase change of the electrodes in the A123 18650 $LiFeO_4$ cell during the over-discharge/charge cycle.

The 1D HESXRD patterns of the A123 18650 $LiFeO_4$ cell at different DODs (10% DOD intervals) of the last charge/over-discharge cycle right before failure are shown in Fig. 7. For this cycle, the diffractogram was recorded from the charge starting with 0% SOC. Once the SOC reached 100%, the over-discharging process was started (from 0% DOD to 120% DOD). In the majority of the diffractograms, eight or more peaks were observed. The expected diffraction peaks (2θ) at 1.21°, 1.44°, 1.78°, 2.06°, and 2.47° were from the 200, 101, 111, 020, and 311 planes of the $LiFePO_4$, the peak (2θ) at 1.25°, 2.53° was from the 200 and 121 planes of the $FePO_4$. The signatures of the two-phase reactions of the $LiFePO_4/FePO_4$ are seen in Fig. 7a for those peaks. In the charging process, the relative intensity of the peaks for $LiFePO_4$ decreased with the increase of the SOC and disappeared at 100% SOC (Fig. 7a), whereas an opposite trend of relative intensity change of the peaks with SOC for the $FePO_4$ was observed.[16] During 20% over-discharge, it was speculated that the Li^+ ions from the electrolyte would be forced to insert into the cathode, which might cause a volume expansion of the cathode, as reflected by the intensity of the $LiFePO_4$ peaks. Comparing the diffractograms of this cell at 100% DOD with those at 120% DOD (Fig. 6b), no obvious changes occurred for either the $LiFePO_4$ or the $FePO_4$ peaks, suggesting that there is no crystalline phase change; hence, the over-insertion of Li^+ ions into the cathode seems unlikely, and the over-discharge seems not to damage the crystalline structure of the cathode. Thus, the damage of the crystal structure of $LiFePO_4$ and $FePO_4$ is not the root cause of failure from over-discharge. The same intensity of these peaks (100% DOD and 120%DOD) before the failure suggests that the $LiFePO_4$ did not decompose.

The structural evolution at the anode side was simultaneously monitored together with that at the cathode side. The diffraction peak at $2\theta = 1.84°$ (Fig. 7c), corresponding to the 002 plane of the graphite showed an interesting change during the charge/over-discharge cycle. The 002 plane peak of the graphite shifted to a smaller angle with increased SOCs (Fig. 7b); due to Li insertion, after 30% SOC, the peak position remained approximately constant at $2\theta = 1.76°$, which is the (002) reflection position expected for a stage-2 LiC_{12}, whereas the relative intensity of the peak decreased as the SOC increased. When SOC reached 100%, the peak for the graphite disappeared, while a new peak at $2\theta = 1.67°$ appeared, which is the (002) reflection of the stage-1 LiC_6. This process was reversed in the discharge process. It is worthwhile to note that the 002 plane peak of the graphite re-appeared at 100% DOD, and when over-discharge continued to 120% DOD, neither the 002 plane peak intensity nor the peak position changed, suggesting that the graphite layer structure was not affected by the over-discharge.

The distance between two neighboring graphite layers, *d*-spacing, can be calculated from the diffraction peak according to the Bragg Equation. The calculated *d*-spacing change over time during the charge and over-discharge cycle is shown in Fig. 7d along with the cell voltage change. Clearly, *d*-spacing increased with SOC during the charge process, corresponding to the insertion of Li^+ ions into the graphite layers. The *d*-spacing decreased as the DOD increased, indicating the de-insertion of Li^+ ions out of the graphite layers. The typical *d*-spacing of the natural graphite for 0% SOC (100% DOD) is 3.354 Å,[17] and the change in the *d*-spacing of the graphite layer during the cycle was within 5% of the standard value. Such a small change of *d*-spacing as that observed in Fig. 6d should not cause a significant increase in cell temperature. Hence, the structural changes of the graphite anode are unlikely the root cause of the failure.

Characterization of the microstructure of the cells.— In order to investigate the morphological changes of the cell components inside

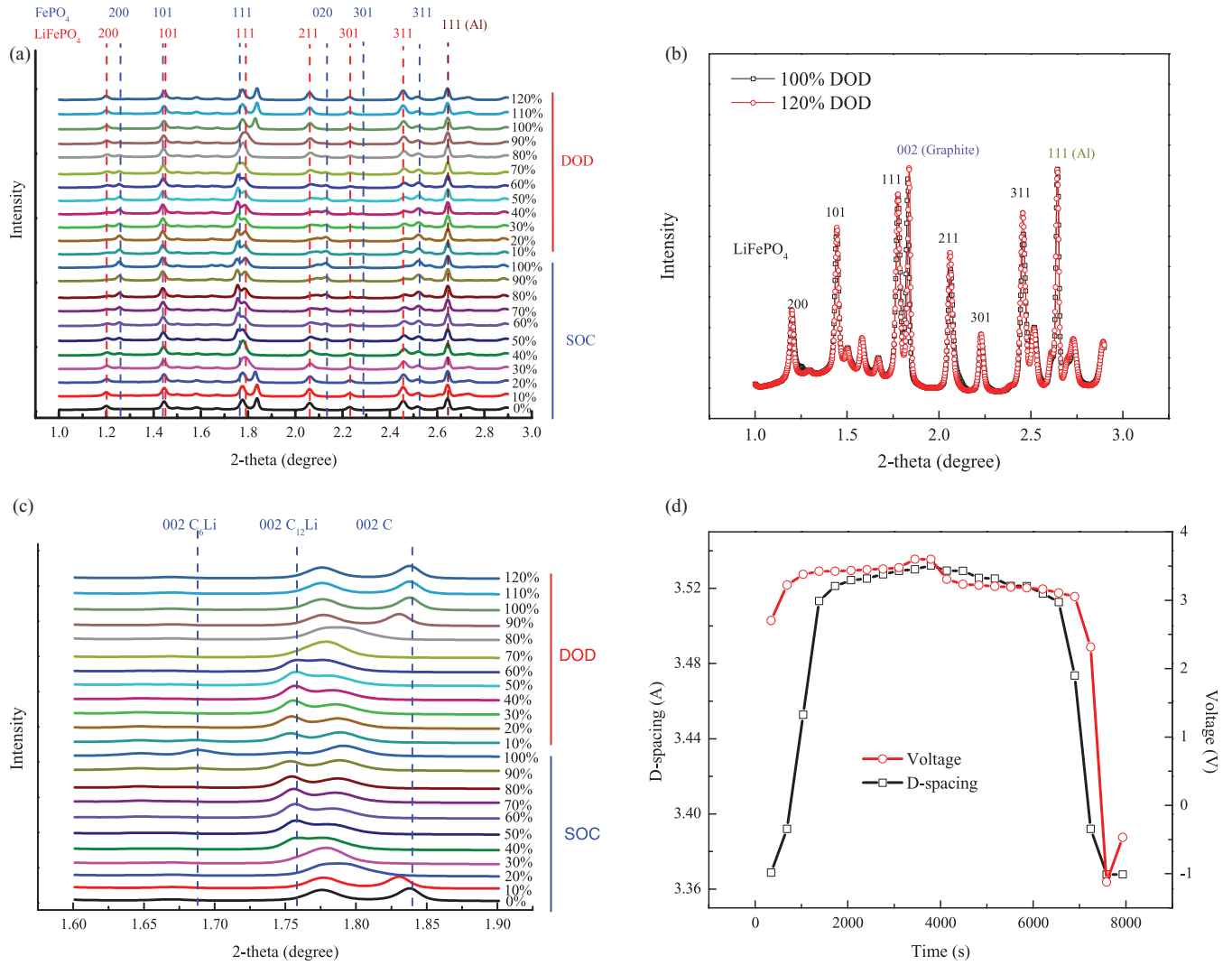

Figure 7. (a) Synchrotron XRD data of an A123 18650 $LiFePO_4$ cell at different SOCs and DODs, (b) comparison of synchrotron XRD data of the cell at DOD = 100% and 120%, (c) graphite peak in the synchrotron XRD data of a $LiFePO_4$ cell and (d) MCMB d-spacing changes of the anode in a $LiFePO_4$ cell during the charge/discharge process.

the cells after the over-discharge process, components in the failed cells were examined using SEM and EDAX. First, the anodes were analyzed. In the anode part, a copper foil was used as the current collector and the two graphite electrode layers sandwiched the copper foil as shown in Fig. 8a. The Cu foil remained in good shape with a smooth surface, and there was no Cu found in the graphite electrode layer as evidenced by EDAX. However, the surface of the Cu foil in the failed cell became rough, and clear corrosion features are seen in Fig. 8b. Furthermore, Cu was found in the graphite electrode layer by EDAX, suggesting that Cu is dissolved from Cu foil and is transferred into the graphite electrode layer. Notice that there is a resin layer on the left hand side of the Cu foil in Fig. 8b because the original graphite electrode layer on the left hand side was detached from the Cu foil after failure, and a resin layer formed when the sample was prepared for SEM analysis.

The separator of the failed cell under 20% over-discharge was examined, and the SEM image is shown in Fig. 9. A number of bright spots on the surface of the separator were observed (as the arrows pointed in Fig. 9a). A closer look (Fig. 9b) reveals that these spots are white deposits, which are Cu, as identified by EDAX (Fig. 9c). Comparing the surface of the separator of the cell cycled under 100% DOD, (Fig. 9d), no such white deposits are observed, and no Cu deposits exist on the surface (Fig. 9e). The Cu was also found inside the separator, as identified by the EDAX, on the cross-section of the separator of the failed cell (Fig. 9f). Similar Cu spots were also found on the opposite side of the separator of the failed cell under 20% over-discharge, suggesting that these spots are Cu dendrites, formed, grown, and penetrated through the separator during the charge/over-discharge cycle.

Similar to the anode, two $LiFePO_4$ cathode electrode layers are sandwiched the aluminum foil of the cathode current collector as shown in Fig. 10a. Both the $LiFePO_4$ cathode electrode layer and the Al foil have a smooth surface and are in good shape. However, after failure, on the outer surface of each $LiFePO_4$ cathode electrode layer, two new layers appear with the outer layer being more dense and the inner layer being more loose, as shown in Fig. 10b (as the arrows indicate). The outer layer (Layer 1 in Fig. 10b) is the resin layer formed during the SEM specimen preparation, as identified by EDAX, which shows a very small amount of Cu but a large amount of C and Cl in this layer (Fig. 10c), while the loose layer (layer 2 in Fig. 10b) with a dense layer (layer 3 in Fig. 10b) on the back is a Cu layer as identified by EDAX (Fig. 10d & 10e). Quite a large amount of Cu is found inside the $LiFePO_4$ cathode electrode layer (Fig. 10f). There is a new layer found on the Al foil surface facing the anode side (layer

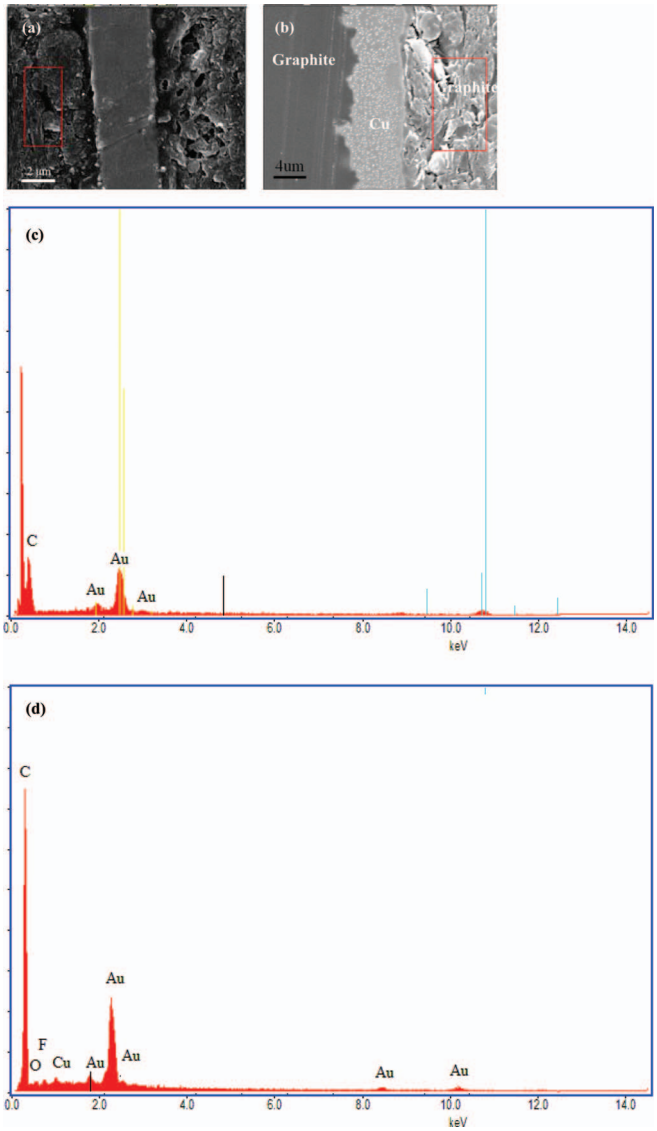

Figure 8. (a) Cross-section SEM image with (c) element distribution of the anode from a fresh cell; (b) cross-section SEM image with (d) element distribution of the anode from a cell that failed after 20% over-discharge cycle.

4 in Fig. 10b) which is a resin layer formed during SEM specimen and identified by EDAX (Fig. 10g) (It was observed that the $LiFePO_4$ cathode electrode layer detached from the Al current collector when the roll of assembly of the 18650 $LiFePO_4$ cell was removed from the case after the failure). Finally, it was found that there was no Cu inside the Al foil, suggesting that the Al-Cu alloy was not formed. To summarize the SEM observation of the cathode, it seems that the Cu ions diffused from the anode side through the separator and eventually reached the cathode. These Cu ions were reduced into a Cu metallic form at the surface of the $LiFePO_4$ cathode electrode layer to form a Cu deposit layer; the rough surface of the layer also demonstrates the formation of the Cu deposit layer and the Cu dendrites. Some of the Cu ions continued to move into the $LiFePO_4$ cathode electrode layer and were reduced into the Cu metallic form inside the cathode electrode layer.

Combining the SEM observation of the anode, the separator, and the cathode, it is clear that the Cu ion is produced from the Cu foil dissolution during the over-discharge process, then these Cu ions migrate toward the cathode and transfer into the separator and, finally, these Cu ions reach the surface of the $LiFePO_4$ cathode electrode layer and are reduced on the surface to form a Cu deposit. Some of the Cu ions move inside the $LiFePO_4$ cathode electrode layer and are reduced. The element distribution of each layer in the fresh and the failed cell is compared in Table I. In the fresh cell, Cu is found only in the anode side, while in the cell that failed under over-discharge conditions, the Cu can be found in the anode, the separator, and the cathode. Other elements remain the same in both the fresh and failed cells. Therefore, from the SEM and EDAX observations, it can be concluded that Cu metal particles formed a bridge between the anode, through the separator, and to the cathode. This bridge could lead to micro-shorting due to the formation of metal dendrites, which can penetrate through the separator and, eventually, could cause the failure of the cell, which is consistent with Hossein's work[7] and Leising's work.[8]

Table I. Element distribution of each layer in fresh and failed cells.

Cells	Parts	Cu	Al	P	O	Fe	C
Fresh	Anode	√					√
	cathode		√	√	√	√	
	separator						√
Failed	Anode	√					√
	cathode	√	√	√	√	√	
	separator	√					√

Failure mechanism.— After systematically studying the behavior of the A123 18650 $LiFePO_4$ cells under over-discharge conditions, characterizing cell components using SEM/EDAX on the failed cells, in-situ monitoring the potential changes and the structural changes of the anode and the cathode using CV and HESXRD, respectively, and electrochemically determining the reduction and oxidation potentials of the Cu for different reactions in the $LiPF_6$/EC-EMC electrolyte system, the possible failure mechanism of an A123 18650 $LiFePO_4$ cell in the charge/over-discharge cycles can be proposed. In an A123 18650 $LiFePO_4$ cell, the copper foil as a current collector on the anode side was oxidized to Cu^+ ions at 3.92 V and continued to be oxidized to Cu^{2+} ions at 4.17 V in the over-discharging process; then, these Cu^{2+} ions diffused to the cathode side driven by the concentration gradient between the anode and the cathode; finally, Cu^{2+} ions were reduced to Cu^+ at 3.28 V and further reduced to Cu metal at 3.19 V at the surface of the cathode $LiFePO_4$ layer in the over-discharge process. The Cu^{2+} ions in the proximity of the cathode simultaneously were reduced to Cu^+ ions and Cu metal to form dendrites because the cathode potential can be as low as 3.16 V in the over-discharge process, which is less than the reduction potential (3.19 V) of $Cu^+ + e^- \rightarrow Cu$. The dendrites will keep growing from the cathode side with charge/discharge cycles, and eventually, the separator will be penetrated through to cause a micro internal short. This is the reason why copper dendrite are the major cause of failure during the over-discharge process rather than during the normal cycle.

Under normal cycle conditions, the anode potential goes up only to 3.80 V, which is below the oxidation potential, 3.92 V ($Cu \rightarrow Cu^+ + 1e^-$) and 4.17 V ($Cu^+ \rightarrow Cu^{2+} + 1e^-$) (Fig. 6d); hence, the dissolution of the copper foil does not occur. In addition, even if there are some Cu ions as impurities existing in the cathode $LiPF_6$ electrode layer, the reduction of the Cu ions to Cu metal cannot take place because the cathode potential can decrease only to 3.28 V, which is much higher than the potential of 3.19 V ($Cu^+ + e^- \rightarrow Cu$) (Fig. 6d). Hence, no Cu dendrite formation occurs for the $LiFePO_4$ cells cycled under normal cycling conditions. This also explains why the $LiFePO_4$ cell can be safely operated at room temperature for 1750 cycles with 80% initial capacity.

Conclusions

The failure of commercial $LiFePO_4$ cells was systematically investigated using commercial A123 18650 cells during

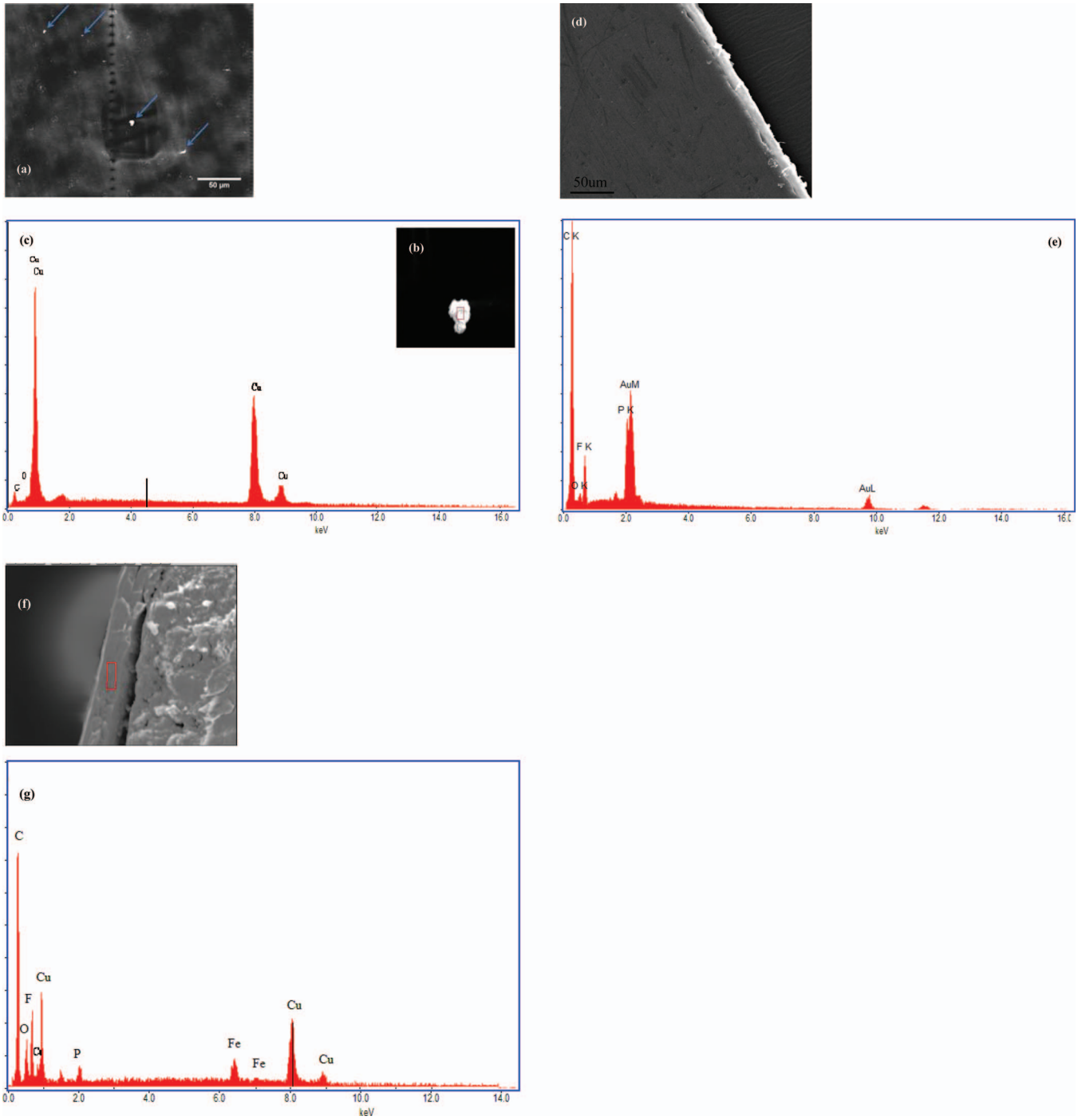

Figure 9. (a) The top-view of SEM image with bright spots of copper bridges (as arrow pointed) formed on the surface of the separator from the cell that failed after a 20% over-discharge cycle; enlarged copper bridge image (b) and EDX (c) of the formed copper bridge; top view (d) and element distribution (e) of the fresh separator; cross-section and element distribution (f) of the failed cell during a 20% over-discharge condition.

charge/over-discharge cycling conditions at a 1 C rate and different degrees of over-discharge (100–120%DOD). The cycle life decreased with the increased degree of over-discharge. Sharp temperature rising during over-discharging process also was observed. Using cyclic voltammetry, the potentials of the Cu/Cu^{+} and Cu/Cu^{2+} oxidation/reduction pairs in 1.2 M $LiPF_6$ in EC-EMC (3:7) were found to be at 3.19 V/3.92 V and 3.28 V/4.17 V, respectively. HESXRD was used to investigate the microstructure changes of the electrodes during the charge and the following over-discharge process. Combining all results, the proposed possible failure mechanism is that the Cu is oxidized into Cu cations on the anode side, then, these Cu cations diffuse through the separator to reach the surface of the cathode and, finally, these Cu cations are reduced to the Cu metallic form at the cathode during the over-discharge process. These Cu deposits grow into Cu dendrites with cycling number and, eventually, they will form the copper bridge that causes micro-shorting. The higher the degree of over-discharge is, the higher the potential of the anode is and, consequently, the more severe the copper dissolution is. This explains the rapid decrease of cycle life of an A123 18650 $LiFePO_4$ cell with an increase in the degree of over-discharge. During normal operation,

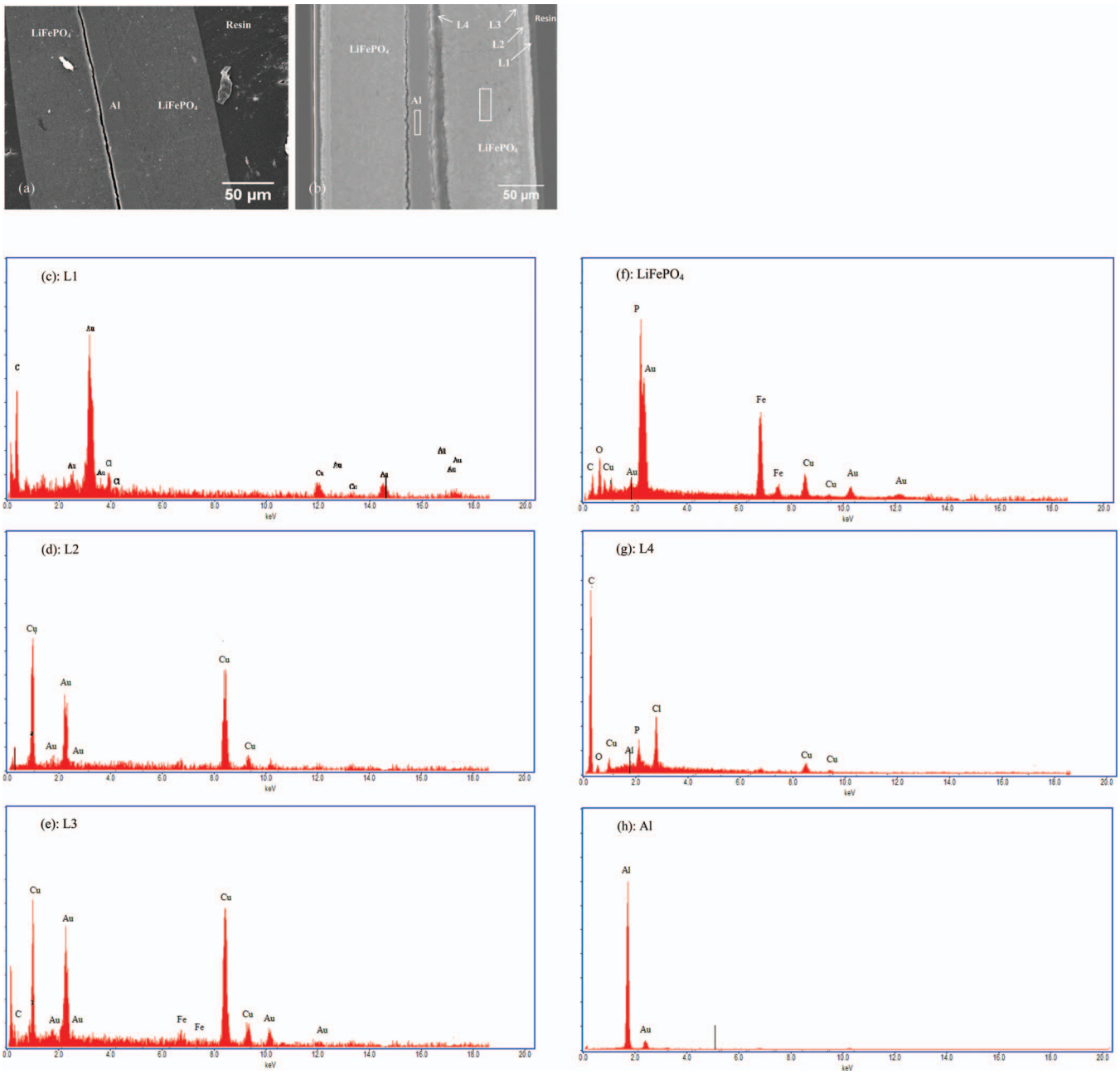

Figure 10. (a) Cross-section SEM image and element distribution of cathode from a fresh cell and (b)a cell that failed during 20% over-discharge cycling. Element distribution of each layer in (b) determined by EDAX: (c) resin layer, L1 in (b); (d) 1st copper layer, L2 in (b); (e) 2nd layer, L3 in (b); (f) $LiFePO_4$ layer in marked rectangular area in (b); (g) resin layer, L4 in (b); (h) Al foil layer in marked rectangular area in (b).

Cu deposition will not occur since the potentials of both the anode and cathode stay in the range outside the Cu oxidation and reduction, which makes the copper foil dissolution and the consequent copper ion reduction into copper metal impossible. The potential changes during the cycle, as well as potentials of the redox couple, explain why the A123 18650 $LiFePO_4$ cells can be safely operated under normal cycling conditions.

Acknowledgments

This work was financially supported by the U.S. Navy under contract N00164-09-C-GS42. The authors would also like to express appreciation to A123 Systems for providing the 18650 LiFePO4 cells for testing. Use of the Advanced Photon Source was supported by the U.S. Department of Energy, Office of Science, Office of Basic Energy Science, under Contract No. DE-AC02-06CH11357.

References

1. M. Stanley Whittingham, *Chem. Rev.*, **104**, 4271 (2004).
2. N. Demirdoven and J. Deutch, *Science*, **305**, 974 (2004).
3. Matthieu Dubarry, Nicolas Vuillaume, and Bor Yann Liaw, *International J. Energy Research*, **34**, 216 (2010).
4. Ben Kenney, Ken Darcovich, Dean D. MacNeil, and Isobel J. Davidson, *J. Power Sources*, **213**, 391 (2012).
5. P. G. Balakrishnan, R. Ramesh, and T. Prem Kumar, *J. Power Sources*, **155**, 401 (2006).
6. Takahisa Ohsaki, Takashi Kishi, Takashi Kuboki, Norio Takami, Nao Shimura, Yuichi Sato, Masahiro Sekino, and Asako Satoh, *J. Power Sources*, **146**, 97 (2005).

7. Hossein Maleki and Jason N. Howard, *J. Power Sources*, **191**, 568 (2009).
8. Randolph A. Leising, Marcus J. Palazzo, Esther Sans Takeuchi, and Kenneth J. Takeuchi, *J. Power Sources*, **681**, 97 (2001).
9. Pankaj Arora and Ralph E. White, *J. Electrochem. Soc.*, **145**, 3647 (1998).
10. Sohrab Hossain, Yong-Kyu Kim, Yousry Saleh, and Raouf Loutfy, *J. Power Sources*, **114**, 264 (2003).
11. Shin-ichi Tobishima, Koji Takei, Yoji Sakurai, and Jun-ichi Yamaki, *J. Power Sources*, **90**, 188 (2000).
12. A. P. Hammersley, S. O. Svensson, M. Hanfland, A. N. Fitch, and D. Häusermann, *High Pressure Res.*, **14**, 235 (1996).
13. Gang Ning, Bala Haran, and Branko N. Popov, *J. Power Sources*, **681**, 160 (2003).
14. Julien Demeaux, Magaly Caillon-Caravanier, Hervé Galiano, Daniel Lemordant, and Bénédicte Claude-Montigny, *J. Electrochem. Soc.*, **159**, A1880 (2012).
15. Fan Xu, Hao He, YaDong Liu, Clif Dun, Yang Ren, Qi Liu, Mei-xian Wang, and Jian Xie, *J. Electrochem. Soc.*, **159**, A1 (2012).
16. H.-H. Chang, C.-C. Chang, H.-C. Wu, M.-H. Yang, H.-S. Sheu, and N.-L. Wu, *Electrochem. Comm.*, **10**, 335 (2008).
17. K. Kinoshita, In *Carbon: Electrochemical and Physiochemical Properties* 1998, John Wiley & Sons.